Title: Beyond Euler/Cardan analysis: True glenohumeral axial rotation during arm elevation and rotation

Running title: True axial rotation of the humerus

Klevis Aliaj, BS[1,2] - klevis.aliaj@utah.edu
K. Bo Foreman, PhD[1,3] - bo.foreman@hsc.utah.edu
Peter N. Chalmers, MD[1] - Peter.Chalmers@hsc.utah.edu
Heath B. Henninger, PhD[1,2,4] - heath.henninger@utah.edu

1 – Department of Orthopaedics, University of Utah, Salt Lake City, UT
2 – Department of Biomedical Engineering, University of Utah, Salt Lake City, UT
3 – Department of Physical Therapy and Athletic Training, University of Utah, Salt Lake City, UT
4 – Department of Mechanical Engineering, University of Utah, Salt Lake City, UT

Corresponding Author:
Heath B Henninger, PhD
University Orthopaedic Center
Orthopaedic Research Laboratory
590 Wakara Way, Rm. A0100
Salt Lake City, UT 84108
Phone: (801) 587-5207
Email: heath.henninger@utah.edu

Submitted to: Gait & Posture
Submitted on: 13 February 2021

Acknowledgements

Research reported in this publication was supported by the National Institute of Arthritis and Musculoskeletal and Skin Diseases (NIAMS) of the National Institutes of Health under award number R01 AR067196. The research content herein is solely the responsibility of the authors and does not necessarily represent the official views of the National Institutes of Health.

Abstract

BACKGROUND: Based on Euler/Cardan analysis, prior investigations have reported up to 80° of glenohumeral (GH) external rotation during arm elevation, which is dependent on the plane of elevation (PoE). However, the subtraction of Euler/Cardan angles does not compute the rotation around the humerus' longitudinal axis (i.e. axial rotation). Clinicians want to understand the true rotation around the humerus' longitudinal axis and rely on laboratory analyses to inform their understanding of underlying shoulder biomechanics – especially for the GH joint since its motion cannot be visually ascertained. True GH axial rotation has not been previously measured *in vivo*, and its difference from Euler/Cardan (apparent) axial rotation is unknown.

RESEARCH QUESTION: What is the true GH axial rotation during arm elevation and external rotation, and does it vary significantly from apparent axial rotation and by PoE?

METHODS: Twenty healthy subjects (10 M/10 F, ages 22-66) were recorded using biplane fluoroscopy while performing arm elevation in the coronal, scapular and sagittal planes, and external rotation in 0° and 90° of abduction. Apparent GH axial rotation was computed using the xz'y'' and yx'y'' sequences. True GH axial rotation was computed by integrating the projection of GH angular velocity onto the humerus' longitudinal axis. One-dimensional statistical parametric mapping was utilized to compare apparent versus true axial rotation, axial rotation versus 0°, and detect differences in axial rotation by PoE.

RESULTS: In contrast to apparent axial rotation, true GH axial rotation does not differ by PoE and is not different than 0° during arm elevation at higher elevation angles. The spherical area between the sequence-specific and actual humeral trajectory explains the difference between apparent and true axial rotation.

SIGNIFICANCE: Proper quantification of axial rotation is important because biomechanics literature informs clinical understanding of shoulder biomechanics. Clinicians care about true axial rotation, which should be reported in future studies of shoulder kinematics.

Keywords: true axial rotation, biplane fluoroscopy, glenohumeral, kinematic analysis

Introduction

Rotation of the humerus about its longitudinal axis, axial rotation, is one of the three primary axes of shoulder motion specified by the International Society of Biomechanics (ISB) [1]. Axial rotation range of motion (ROM) is critical in performing activities of daily living, and therefore is routinely measured by clinicians [2]. Beyond ROM, axial rotation is a key component to understanding how the synchronized multiaxial rotations of the sternoclavicular, acromioclavicular, scapulothoracic (ST), and glenohumeral (GH) joints produce smooth, pain-free shoulder motion [3]. Axial rotation can induce GH joint capsule twisting [4], which likely contributes to shoulder motion and stability, and is thus important for sport science investigations [5]. Patients with rotator cuff tears lose axial rotation ROM and strength [6], and these deficits may persist even after surgical treatment (e.g. reverse total shoulder arthroplasty) [7, 8]. Due to the central role of humerus axial rotation in human motion and investigating disease progression, accurate and consistent quantification is critical.

In a clinical setting, axial rotation is commonly measured in the transverse and sagittal planes (Fig. 1). Researchers can measure axial rotation during compound 3D motions, and is predominantly calculated from Euler/Cardan angles, although its computation is subject to debate [1, 9-13]. Euler/Cardan decompositions are equivalent to the globe coordinate system [14, 15]. The third rotation axis is customarily utilized to determine humeral axial orientation [1, 9, 10], with the forearm as a visual indicator of orientation. Although the distal humerus traces an irregular path along the globe, Euler/Cardan decompositions force it to travel strictly along the latitudes and longitudes, and the forearm to stay tangent to longitudes/latitudes [14] (Fig. 2). We term this artificially imposed path a *sequence-specific trajectory*. Herein, sequence-specific

axial orientation denotes the last component of a decomposition; sequence-specific *apparent axial rotation* is computed by subtracting two axial orientations; and *true axial rotation* denotes the actual rotation that occurs about the humerus' longitudinal axis [12]. True axial rotation is computed by integrating the projection of GH angular velocity onto the humerus' longitudinal axis [12]. Subtracting Euler/Cardan angles to obtain the rotation between two orientations is a common practice even though it is mathematically incorrect [16, 17]. Subtraction of the first two Euler angles does not compute a rotation, but it does quantify changes in latitude/longitude along the globe [18] – which has physical meaning. However, no physical interpretation can be attributed to subtraction of the 3rd Euler/Cardan angle, hence termed *apparent* axial rotation.

The difference between apparent and true axial rotation is evident in Codman's paradox as explained by both Miyazaki [12] and Pearl: "When the arm traces out any closed path on the surface of a sphere without rotation about its [longitudinal] axis, an induced change occurs in the [axial] orientation that is equal to the area enclosed by the path of the motion" [19]. Thus, the induced change in axial orientation (and apparent axial rotation) does not occur because of a physical rotation around the longitudinal axis, but simply because of changes in latitude/longitude (i.e. elevation/PoE, Fig. 2). Apparent axial rotation is pervasive in the literature [3, 20-22], even though it does not represent a physical rotation around the humerus' longitudinal axis and impedes comparison between studies. Prior studies have reported up to 80° of apparent GH external rotation that depends on the PoE [3, 21]. However, other studies have shown slight internal rotation and that the choice of decomposition sequence greatly affects axial rotation [20]. True axial rotation has not been previously measured *in-vivo* in a healthy population for clinically relevant motions. Proper quantification of axial rotation is important

because biomechanics literature [3] informs both clinical understanding of shoulder biomechanics and textbook content [2], especially for the GH joint since its motion cannot be visually ascertained.

In this investigation we analyzed true GH axial rotation and examined its difference from apparent GH axial rotation, for coronal plane abduction (CA), scapular plane abduction (SA), forward elevation (FE), external rotation in adduction (ER-ADD, Fig. 1A) and external rotation at 90° of abduction (ER-ABD, Fig. 1B). Based on observing the rotation around the humerus' longitudinal axis of GH animations created from biplane fluoroscopy, we hypothesized that 1) true GH axial rotation is zero during arm elevation for all PoE, 2) true, unlike apparent, GH axial rotation is not dependent on the PoE, 3) true GH axial rotation is significantly different than two common sequences (yx'y'', xz'y'') of apparent axial rotation during arm elevation, 4) for external rotation trials, the only difference between true and apparent axial rotation is for the yx'y'' sequence during ER-ADD.

The swing-spin [11] (tit-torsion [13]) decomposition, which has been proposed to provide a more natural representation of axial rotation, was also examined. In the swing-spin decomposition the humerus' orientation is established in two steps: 1) a rotation aligns the humerus' longitudinal axis from its neutral anatomical direction to its final direction (swing) – establishing both the PoE and elevation angle, and 2) a rotation around the longitudinal axis of the humerus establishes axial orientation (spin) [11, 13]. The PoE and elevation angle are equivalent between the yxy'' sequence and the swing-spin decomposition [13]. However, the swing-spin axial orientation is equivalent to adding the PoE and axial orientation from the ISB-recommended yx'y'' sequence [13].

Methods

The present analysis was performed on kinematic data previously collected in a study of healthy shoulder kinematics [23, 24]. Briefly, after obtaining informed consent (IRB 71782), twenty healthy subjects (10M/10F; 42±17 yrs; 172.3±8.8 cm; 69.9±15.7 kg; right-hand dominant) had the motion of their right humerus and scapula imaged at 100 Hz using a custom biplane fluoroscopy system (Radiological Imaging Services, Hamburg, PA). The position of reflective markers on the torso were recorded at 100 Hz using a ten-camera motion analysis system (Vicon Motion Systems, Oxford, UK). For elevation trials, subjects were instructed to elevate their right arm with the elbow fully extended and hand in the thumb up position at approximately 60°-90° per second. Elevation was performed in the coronal, scapular (30° anterior to coronal plane), and sagittal planes. For ER-ADD, subjects were instructed to maintain the elbow by their torso with the hand on the abdomen and thumb pointing up, and laterally rotate to their full ROM at ~45°/sec (Fig. 1A). For ER-ABD, subjects were instructed to point their elbow towards their side while allowing the hand to hang naturally due to its weight, and laterally rotate up to their full ROM at ~45°/sec (Fig. 1B).

3D models of the humerus and scapula were constructed from each subject's CT scan. Model-based markerless tracking ascertained the 3D position and orientation of each bone model by semi-automatically aligning digitally reconstructed radiographs against each frame of the biplane fluoroscopy recordings [25, 26] . Anatomical coordinate systems of the humerus, scapula, and torso followed ISB recommendations [1] except that the glenoid center defined the lateral axis of the scapula. Utilizing the acromial angle excluded 4 trials due to humerus orientations reaching singularity (Appendix 2).

One subject (F, 51 years) was excluded from the analysis based on visual evidence of not establishing the thumb-up position at the beginning of the capture. The FE trial for one subject (M, 27 years) was excluded due a recording gap at the beginning of the trial. Humerothoracic (HT) elevation ROM of 25-130° was achieved by all included subjects/trials and was used for subsequent analysis. GH orientation trajectories were smoothed using a 7-frame moving-average quaternion filter [27]. GH orientation trajectories were interpolated in the 25-130° range every 0.25 degrees using spherical linear interpolation [28]. Because minimal elevation occurs during ER-ADD and ER-ABD trials, they were instead interpolated at 0.25% increments between the start (0%) of the motion and maximum external rotation (100%). Axial orientation was quantified using the yx'y'' Euler sequence as prescribed by ISB [1] and the xz'y'' Cardan sequence. The xz'y'' sequence overcomes the numerical instability of yx'y'' when the humerus is in adduction [10]. Apparent axial rotation was computed by subtracting the axial orientation at the start of the motion from all subsequent timepoints. Letting a_0 and p_0 represent axial orientation and PoE at the start of the motion, respectively, and a_k and p_k represent the same at time *k*, swing spin axial rotation was computed as: $(a_k + p_k) - (a_0 + p_0)$.

The angular velocity vector was extracted by computing the angular velocity tensor from GH orientation trajectories [29]. True GH axial rotation was computed by projecting GH angular velocity onto the humerus' longitudinal axis and numerically integrating (trapezoidal rule) Equation (1) from the start of the motion to each timepoint in the motion capture [12] (Appendix 3 also presents alternate methods). Let $\theta(t_k)$ represent true axial rotation at time t_k, ${}^S\boldsymbol{\omega}(t_k)$ represent GH angular velocity in the scapula's frame and ${}^S\mathbf{l}(t_k)$ represent the humerus' longitudinal axis in the scapula's frame. True axial rotation was computed as:

$$\theta(t_k) = \int_0^{t_k} {}^S\boldsymbol{\omega} \cdot {}^S\mathbf{l}\, dt \tag{1}$$

To ascertain integration drift due to linearization, GH trajectories computed from integrating the angular velocity vector [30] were compared against the original GH trajectories [31]. For each trajectory, the maximum difference was analyzed and did not reveal appreciable drift: 0.13°±0.04° (maximum drift for all trajectories and all timepoints was 0.36°).

One-dimensional statistical parametric mapping (SPM1D [32]) was utilized to: compare apparent axial rotation against true axial rotation (non-parametric, paired t-test) for all trials; compare GH axial rotation against the null hypothesis of 0° (non-parametric t-test) for elevation trials; detect differences in axial rotation between planes of elevation (one-way, repeated-measured (RM), ANOVA). A significance level of 0.05 was utilized for all statistical tests. Since one FE trial was excluded due to a recording gap, the corresponding CA and SA trials for the same subject were excluded from the RM-ANOVA tests.

The supporting dataset and code repository for all analyses are located at https://doi.org/10.5281/zenodo.4536683 and https://doi.org/10.5281/zenodo.4538959, respectively.

Results

GH true axial rotation did not differ from zero beyond 100° of HT elevation for CA, beyond 83° of HT elevation for SA, and for all HT elevations angles for FE. At maximum HT elevation, GH true axial rotation was -5.7°±11.5° for CA, -4.2°±16.1° for SA, and 0.8°±12.9° for FE (Fig. 3D). True axial rotation did not differ between CA, SA, and FE. In contrast, there were differences between the three planes of elevation for xz'y'' apparent axial rotation beyond 45° of HT elevation, for all HT elevation angles for yx'y'', and for HT elevation angles <78° and >128° for the swing-spin decomposition (Fig. 3E-G).

The xz'y'' GH apparent axial rotation differed from true axial rotation for HT elevations >50° for CA, <29° and >91° for SA, and for all elevation angles for FE (Fig. 4A-C). At maximum HT elevation, the mean difference between xz'y'' apparent and true axial rotation was 25.7°, 12.8°, and -28.9° for CA, SA, and FE, respectively. The yx'y'' sequence differed from true axial rotation for all HT elevation angles for CA and SA but did not differ for FE (Fig. 4D-F). At maximum HT elevation, the mean difference between yx'y'' apparent and true axial rotation was 30.1°, 27.2°, and -3.9° for CA, SA, and FE, respectively. The swing-spin decomposition differed from true axial rotation for HT elevation angles <120° for CA, <128° for SA and >95° for FE. At maximum HT elevation, the mean difference between swing-spin apparent and true axial rotation was 11.8°, 4.9°, and -30.0° for CA, SA, and FE, respectively.

During ER-ABD, xz'y'' GH apparent axial rotation was different than true axial rotation beyond 70% of motion completion (Fig. 5B). No other statistical differences between true and apparent axial rotation were found during ER-ABD and ER-ADD. At maximum external rotation, the mean difference between xz'y'' apparent and true axial rotation was 0.2° and -5.5° for ER-

ADD and ER-ABD, respectively (Fig. 5A-B). For yxy'' these differences were -2.5° and 0.7° and for swing-spin they were -0.7° and -2.2° (Fig. 5C-D).

Discussion

This investigation demonstrates that for arm elevation trials, true GH axial rotation is not significantly different than 0° beyond ~90° of HT elevation and does not vary by PoE (Fig. 3D). In contrast, prior Euler/Cardan analyses have reported apparent rotations from 5° of internal rotation up to 80° of external rotation that varies by PoE [3, 20, 21]. The large variability in prior axial rotation measurements is a consequence of the chosen decomposition sequences and provides limited insight into *in-vivo* GH joint kinematics. Our findings extend to other investigations. We computed true axial rotation from the mean GH trajectories published by Ludewig et al. and found that 1) true axial rotation converges between different PoE, while xz'y'' apparent axial rotation diverges, and 2) at 120° of HT elevation the average true external axial rotation is at most 25° compared to 50° for apparent axial rotation (Appendix 4). This is notable because it would likely change the author's conclusion that axial rotation varies by PoE and it may have changed the author's conclusion that elevation is associated with external GH axial rotation (depending on subject-specific variability).

For all trials examined, the difference between true and apparent axial rotation could be predicted numerically to within 0.1° based on the closed path created by the actual and sequence-specific humeral trajectory [19, 33] (Fig. 2, data not shown, see code repository). The difference between xz'y'' and true axial rotation is specified completely by the spherical area between the sequence-specific and actual humeral trajectory (Fig. 2A). In general, the spherical area increases in width from SA to CA to FE. Accordingly, apparent axial rotation will diverge from true axial rotation at higher elevation angles for SA and lower elevation angles for FE, with CA falling between (Fig. 4). For ER-ABD, xz'y'' is significantly different than true axial rotation beyond

70% of motion completion, contrary to our hypothesis (Fig. 5). We assumed that the distal humerus remained stationary during ER-ABD, and hence the enclosed spherical area was negligible. But there was enough distal humerus movement to cause deviations from true axial rotation, although at maximum external rotation this difference was only ~5°.

To explain the difference between yx'y'' and true axial rotation, it is necessary to account for both the enclosed spherical area and the difference in the PoE from the start of the motion, since axial rotation of the humerus is utilized to establish the PoE (Appendix 1). To demonstrate this, imagine a subject performing CA with the forearm pointing anteriorly. Because of body habitus, the subject may be slightly elevated in the sagittal plane at the start of the motion resulting in the humerus being at 90° of external axial orientation (Fig. 6). As the subject elevates in the coronal plane, with the forearm still pointing anteriorly, the subject will arrive at 0° of axial orientation, which explains how changes in the PoE contribute to apparent axial rotation. The changes in PoE may be associated with body habitus or with numerical instability in computing the PoE while the arm is near the resting position [10]. This guided our hypothesis that yx'y'' axial rotation is different than true axial rotation for ER-ADD. Indeed, there are large changes in yx'y'' axial rotation for ER-ADD (Fig. 5) for individual subjects, but the means were unchanged.

Large changes in PoE account for the characteristic large changes in axial rotation (both GH and HT) at the start of elevation trials seen herein (Appendix 5) and in prior studies [20-22]. In our analysis, the HT elevation range of 0°-25° accounted for up to 40% of changes in yx'y'' GH apparent axial rotation (Fig. 3, 4). Furthermore, the yx'y'' axial rotation changes at the start of elevation trials vary widely by subject (Appendix 5), leading to increased variability when utilizing the yx'y'' sequence. This reduces the power of statistical tests to distinguish between different

groups (e.g. normal versus pathological). The increased variability is magnified when utilizing the ISB recommended acromial angle to establish the lateral direction of the scapula (Appendix 2). In contrast, true axial rotation is not affected by the anatomical landmarks used to establish the scapular coordinate system (Appendix 6).

It is instructive and useful to account for the changes in axial rotation caused by changes in PoE for the yx'y'' sequence. The swing-spin decomposition – previously proposed to provide a more natural representation of axial rotation [11, 13] – accomplishes this exact objective because the swing-spin axial orientation is equivalent to adding the PoE and axial orientation from the yx'y'' sequence [13]. Qualitatively, swing-spin agrees with true axial rotation more closely than yx'y'' (Fig. 4, 5). However, past ~130° of HT elevation for CA and SA, and past ~100° of HT elevation for FE, swing-spin deviates sharply from true axial rotation. This can be explained by the large increase in spherical area for the yx'y'' decomposition past the aforementioned HT elevation angles (Fig. 2). The typical yx'y'' decomposition does not suffer from the same sharp changes in axial rotation at higher HT angles because changes in spherical area are balanced by changes in PoE.

Although apparent can vary from true GH axial rotation in subtle ways, the following statements will largely hold true: 1) xz'y'' axial rotation most closely resembles true axial rotation for PoEs close to the scapular plane and at lower HT angles, 2) swing-spin should be favored over normal yx'y'' axial rotation when interpreting prior studies for HT elevation angles lower than 130° for CA and SA, and lower than 100° for FE, and 3) for ER-ABD and ER-ADD either xz'y'' or swing-spin axial rotation may be utilized. The swing-spin axial rotation works well even when the acromial angle is utilized (Appendix 2) and when analyzing HT axial rotation (Appendix 7).

This investigation demonstrates that true axial rotation should be computed during kinematic analysis to both mathematically and physically quantify axial rotation correctly. Because true axial rotation quantifies the actual rotation around the humerus' longitudinal axis, it is a quantity that closely aligns with a clinician's expectation of axial rotation [34]. Apparent axial rotation should be avoided because it differs from true axial rotation based on decomposition sequence and PoE, and it is subject to numerical instabilities. These effects are compounded when considering multiplanar movements because the spherical area between the actual and sequence-specific trajectory is magnified. Although the spherical area explains the difference between apparent and true axial rotation, true axial rotation can be efficiently computed from angular velocity as defined by Miyazaki et al. [12] (Appendix 3). This definition elucidates that true axial rotation is a scalar (zero-order tensor) coordinate-system invariant quantity which depends only on the definition of the humerus' longitudinal axis and is not affected by the anatomical coordinate system of the scapula (Appendix 6). Furthermore, unlike apparent axial rotation, true axial rotation is not affected by singularities.

True axial rotation complements the globe coordinate system. Changes in longitude/latitude determine changes in the direction of the longitudinal axis, and true axial rotation measures the rotation about the longitudinal axis. Because true axial rotation is a path-dependent quantity [12] it accounts for how a motion is performed, making it a good candidate for exploring compensatory kinematic patterns. However, true axial rotation does not measure axial orientation: a motion trajectory is necessary to compute angular velocity and perform integration. Euler/Cardan angles can be utilized to quantify axial orientation. For example, the yx'y'' sequence provides a simple measure of axial orientation by quantifying the elbow axis angle

against a horizontal plane. However, caution must be exercised when presenting axial orientation plots because – at least in biomechanics – the changes conveyed in these plots are (incorrectly) associated with axial rotation [16]. Furthermore, Euler/Cardan angles fail to provide a consistent axial orientation measure against an axis because 0° of axial orientation varies based on the position of the distal end of the humerus on the globe (Fig. 6). Further research is necessary to determine a method for measuring axial orientation consistently, especially when analyzing goal-oriented tasks/poses.

The benefits of using true, rather than apparent, axial rotation are numerous and it should be the preferred method of computing axial rotation. Most importantly, it measures the actual rotation around the longitudinal axis of the humerus. This is a quantity that clinicians easily intuit and is useful in understanding the kinematics of the shoulder joint. To increase reproducibility and ease the transition to true axial rotation, this manuscript is accompanied by a data and code repository that includes Python, MATLAB, and Visual3D functions for computing true axial rotation.

References

[1] G. Wu, F.C. van der Helm, H.E. Veeger, M. Makhsous, P. Van Roy, C. Anglin, et al., ISB recommendation on definitions of joint coordinate systems of various joints for the reporting of human joint motion--Part II: shoulder, elbow, wrist and hand, Journal of biomechanics 38(5) (2005) 981-992.
[2] C.C. Norkin, D.J. White, Measurement of joint motion: a guide to goniometry, FA Davis2016.
[3] P.M. Ludewig, V. Phadke, J.P. Braman, D.R. Hassett, C.J. Cieminski, R.F. LaPrade, Motion of the shoulder complex during multiplanar humeral elevation, The Journal of bone and joint surgery. American volume 91(2) (2009) 378-89.
[4] J.E. Novotny, B.D. Beynnon, C.E. Nichols Iii, A numerical solution to calculate internal–external rotation at the glenohumeral joint, Clinical Biomechanics 16(5) (2001) 395-400. http://www.sciencedirect.com/science/article/pii/S0268003301000183.
[5] R.N. Marshall, B.C. Elliott, Long-axis rotation: the missing link in proximal-to-distal segmental sequencing, Journal of sports sciences 18(4) (2000) 247-54.
[6] L.C. Hall, E.E. Middlebrook, C.R. Dickerson, Analysis of the influence of rotator cuff impingements on upper limb kinematics in an elderly population during activities of daily living, Clinical Biomechanics 26(6) (2011) 579-584. http://www.sciencedirect.com/science/article/pii/S0268003311000441.
[7] T.D.W. Alta, H.E.J. Veeger, T.W.J. Janssen, W.J. Willems, Are Shoulders with A Reverse Shoulder Prosthesis Strong Enough? A Pilot Study, Clinical Orthopaedics and Related Research® 470(8) (2012) 2185-2192. https://doi.org/10.1007/s11999-012-2277-8.
[8] J.L. Berliner, A. Regalado-Magdos, C.B. Ma, B.T. Feeley, Biomechanics of reverse total shoulder arthroplasty, Journal of Shoulder and Elbow Surgery 24(1) (2015) 150-160. http://www.sciencedirect.com/science/article/pii/S1058274614004509.
[9] C.A. Doorenbosch, J. Harlaar, D.H. Veeger, The globe system: an unambiguous description of shoulder positions in daily life movements, Journal of rehabilitation research and development 40(2) (2003) 147-55.
[10] V. Phadke, J.P. Braman, R.F. LaPrade, P.M. Ludewig, Comparison of glenohumeral motion using different rotation sequences, Journal of biomechanics 44(4) (2011) 700-5.
[11] P.L. Cheng, A.C. Nicol, J.P. Paul, Determination of axial rotation angles of limb segments — a new method, Journal of biomechanics 33(7) (2000) 837-843. http://www.sciencedirect.com/science/article/pii/S0021929000000324.
[12] S. Miyazaki, A. Ishida, New mathematical definition and calculation of axial rotation of anatomical joints, Journal of biomechanical engineering 113(3) (1991) 270-5.
[13] A. Campeau-Lecours, D.-S. Vu, F. Schweitzer, J.-S. Roy, Alternative Representation of the Shoulder Orientation Based on the Tilt-and-Torsion Angles, Journal of biomechanical engineering 142(7) (2020). https://doi.org/10.1115/1.4046203.
[14] R. Baker, Globographic visualisation of three dimensional joint angles, Journal of biomechanics 44(10) (2011) 1885-91.
[15] G.T. Rab, Shoulder motion description: The ISB and Globe methods are identical, Gait & posture 27(4) (2008) 702-705. http://www.sciencedirect.com/science/article/pii/S0966636207001762.
[16] R. Krishnan, N. Bjorsell, E.M. Gutierrez-Farewik, C. Smith, A survey of human shoulder functional kinematic representations, Med Biol Eng Comput 57(2) (2019) 339-367.
[17] B. Michaud, M.I. Jackson, F. Prince, M.S. Begon, Can one angle be simply subtracted from another to determine range of motion in three-dimensional motion analysis?, Computer methods in biomechanics and biomedical engineering 17(5) (2014) 507-15.
[18] P.L. Cheng, Joint rotation between two attitudes in the spherical rotation coordinate system, Journal of biomechanics 37(10) (2004) 1475-1482. http://www.sciencedirect.com/science/article/pii/S0021929004000508.

[19] M.L. Pearl, J.A. Sidles, S.B. Lippitt, D.T. Harryman, 2nd, F.A. Matsen, 3rd, Codman's paradox: Sixty years later, J Shoulder Elbow Surg 1(4) (1992) 219-25.
[20] K. Matsuki, K.O. Matsuki, S. Yamaguchi, N. Ochiai, T. Sasho, H. Sugaya, et al., Dynamic in vivo glenohumeral kinematics during scapular plane abduction in healthy shoulders, The Journal of orthopaedic and sports physical therapy 42(2) (2012) 96-104.
[21] C.G.M. Meskers, H.M. Vermeulen, J.H. de Groot, F.C.T. van der Helm, P.M. Rozing, 3D shoulder position measurements using a six-degree-of-freedom electromagnetic tracking device, Clinical Biomechanics 13(4) (1998) 280-292. http://www.sciencedirect.com/science/article/pii/S0268003398000953.
[22] M. Stokdijk, P.H.C. Eilers, J. Nagels, P.M. Rozing, External rotation in the glenohumeral joint during elevation of the arm, Clinical Biomechanics 18(4) (2003) 296-302. http://www.sciencedirect.com/science/article/pii/S0268003303000172.
[23] C.W. Kolz, H.J. Sulkar, K. Aliaj, R.Z. Tashjian, P.N. Chalmers, Y. Qiu, et al., Age-related differences in humerothoracic, scapulothoracic, and glenohumeral kinematics during elevation and rotation motions, Journal of biomechanics 117 (2021) 110266. http://www.sciencedirect.com/science/article/pii/S0021929021000464.
[24] C.W. Kolz, H.J. Sulkar, K. Aliaj, R.Z. Tashjian, P.N. Chalmers, Y. Qiu, et al., Reliable interpretation of scapular kinematics depends on coordinate system definition, Gait & posture 81 (2020) 183-190. http://www.sciencedirect.com/science/article/pii/S0966636220302617.
[25] M.J. Bey, R. Zauel, S.K. Brock, S. Tashman, Validation of a new model-based tracking technique for measuring three-dimensional, in vivo glenohumeral joint kinematics, Journal of biomechanical engineering 128(4) (2006) 604-609. https://www.ncbi.nlm.nih.gov/pubmed/16813452.
[26] A.L. Kapron, S.K. Aoki, C.L. Peters, S.A. Maas, M.J. Bey, R. Zauel, et al., Accuracy and feasibility of dual fluoroscopy and model-based tracking to quantify in vivo hip kinematics during clinical exams, Journal of applied biomechanics 30(3) (2014) 461-470. https://pubmed.ncbi.nlm.nih.gov/24584728.
[27] F.L. Markley, Y. Cheng, J.L. Crassidis, Y. Oshman, Averaging quaternions, Journal of Guidance, Control, and Dynamics 30(4) (2007) 1193-1197.
[28] K. Shoemake, Animating rotation with quaternion curves, Proceedings of the 12th annual conference on Computer graphics and interactive techniques, 1985, pp. 245-254.
[29] D. Condurache, M. Matcovschi, Computation of angular velocity and acceleration tensors by direct measurements, Acta Mechanica 153(3) (2002) 147-167. https://doi.org/10.1007/BF01177449.
[30] M. Boyle, The integration of angular velocity, Advances in Applied Clifford Algebras 27(3) (2017) 2345-2374.
[31] D.Q. Huynh, Metrics for 3D Rotations: Comparison and Analysis, Journal of Mathematical Imaging and Vision 35(2) (2009) 155-164. https://doi.org/10.1007/s10851-009-0161-2.
[32] T.C. Pataky, J. Vanrenterghem, M.A. Robinson, Zero- vs. one-dimensional, parametric vs. non-parametric, and confidence interval vs. hypothesis testing procedures in one-dimensional biomechanical trajectory analysis, Journal of biomechanics 48(7) (2015) 1277-1285. http://www.sciencedirect.com/science/article/pii/S0021929015001438.
[33] Y.-S. Yoon, Enumeration of Axial Rotation, Advances in Biomechanics and Applications 1(2) (2014) 85-93.
[34] V.M. Zatsiorsky, Kinematics of Human Motion, Human Kinetics1998.

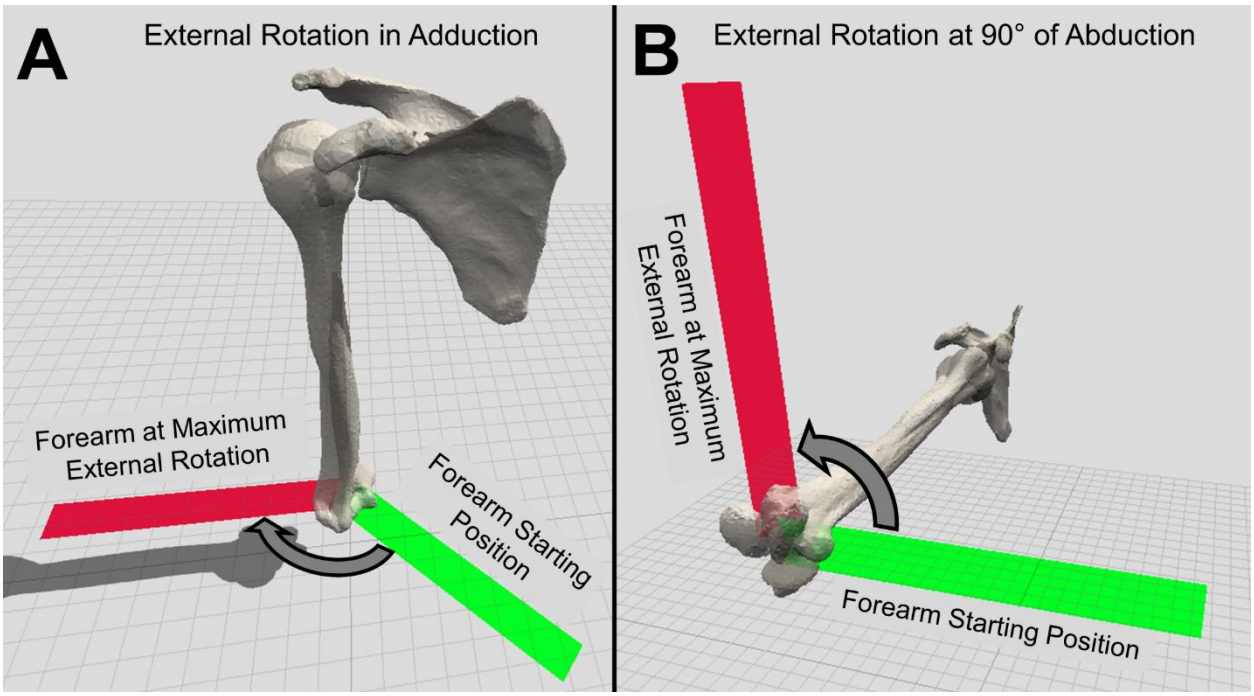

Fig. 1: Graphical depiction of external rotation in the transverse plane (**A**, External Rotation in Adduction, ER-ADD) and external rotation in the sagittal plane (**B**, External Rotation at 90° of Abduction, ER-ABD). For ER-ADD trials, subjects were instructed to maintain the elbow by their torso with the hand on the abdomen and thumb pointing up, and to laterally rotate to their full ROM at ~45°/sec. For ER-ABD trials, subjects were instructed to point their elbow towards the side of the room while allowing the hand to hang naturally due to its weight, and laterally rotate up to their full ROM at ~45°/sec. Green lines denote the starting position of the forearm axis, and red lines denote the ending position of the forearm axis.

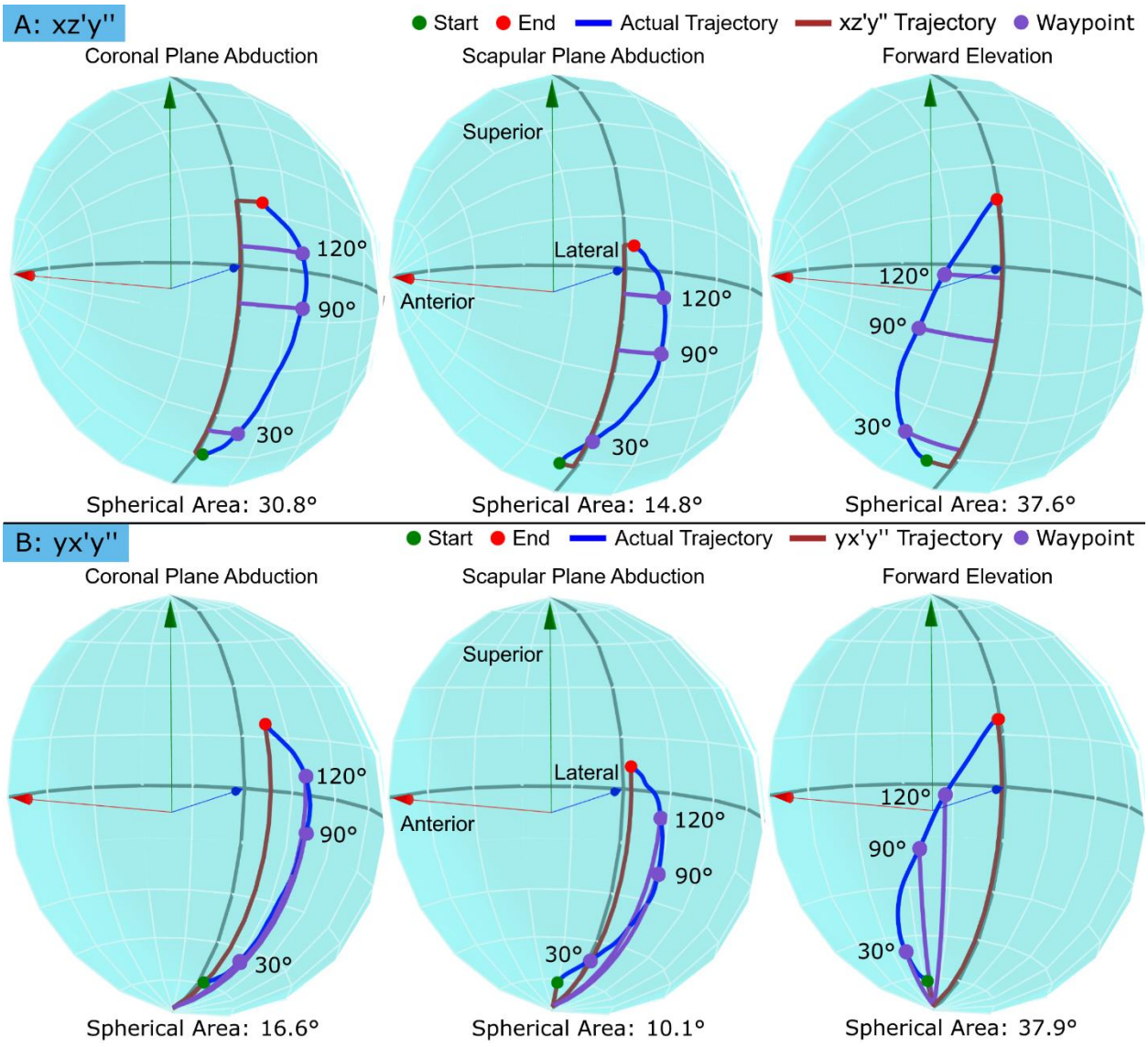

Fig. 2: Spherical area illustrations for arm elevation motions. The xz'y'' (**A**) and the yx'y'' (**B**) decompositions yield the sequence-specific humeral trajectory (brown), where the actual humeral trajectory (blue) is shown for coronal plane abduction (left), scapular plane abduction (middle), and forward elevation (right). Apparent GH axial rotation is computed by following the sequence-specific humeral trajectory, while true GH axial rotation is computed by following the actual humeral trajectory. The spherical area encompassed between the two trajectories represents the absolute value of the difference between apparent and true axial rotation. Appendix 1 details how the paths were constructed. The position of the distal humerus on the sphere at 30°, 90°, and 120° of HT elevation is indicated on the sphere to demonstrate how the spherical area changes with increased HT elevation angles.

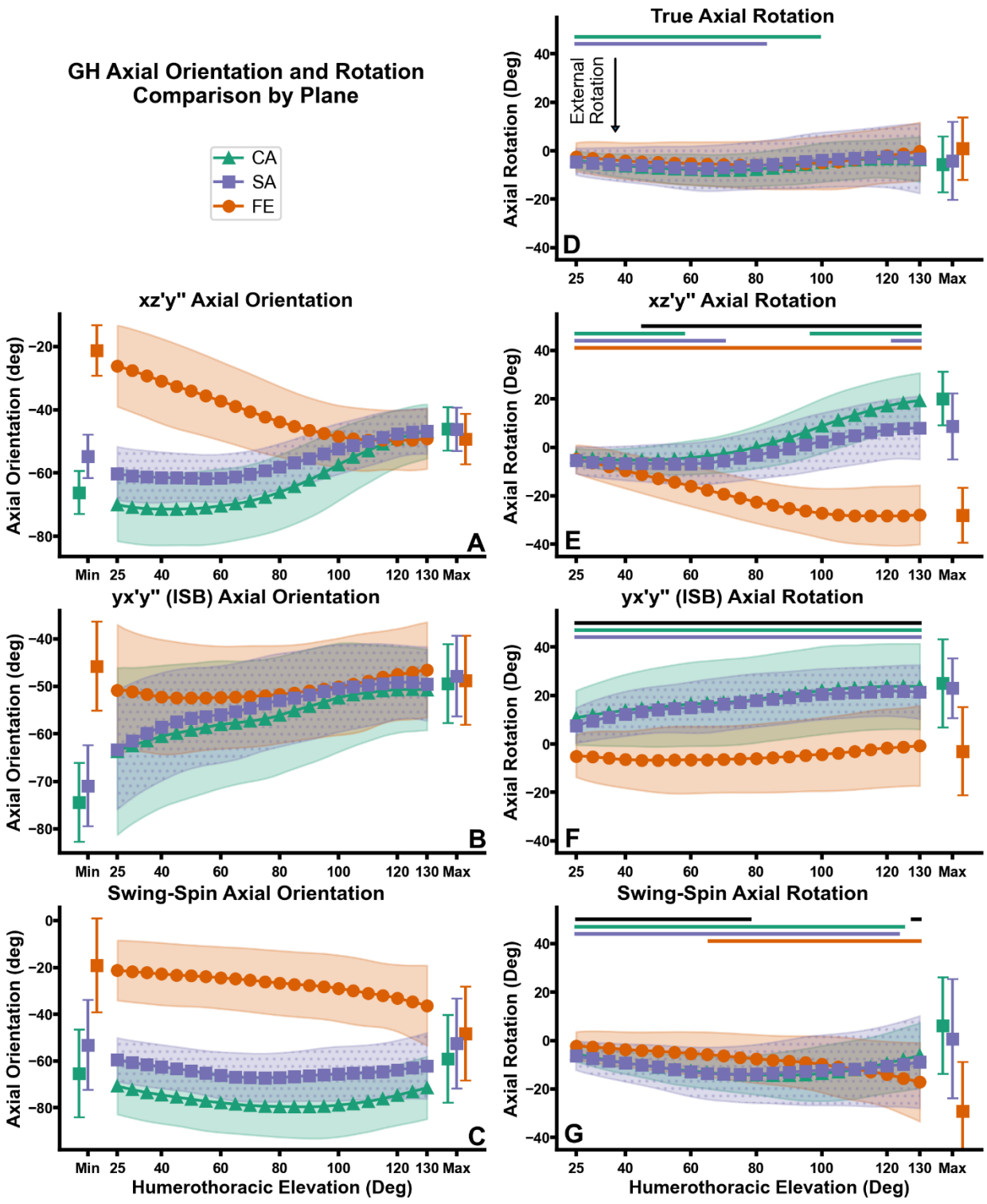
GH Axial Orientation and Rotation Comparison by Plane
CA
SA
FE
True Axial Rotation
External Rotation
Axial Rotation (Deg)
D
xz'y'' Axial Orientation
Axial Orientation (deg)
A
xz'y'' Axial Rotation
E
yx'y'' (ISB) Axial Orientation
B
yx'y'' (ISB) Axial Rotation
F
Swing-Spin Axial Orientation
C
Swing-Spin Axial Rotation
G
Min 25 40 60 80 100 120 130 Max
Humerothoracic Elevation (Deg)

Fig. 3: Comparison between the coronal, scapular, and sagittal planes of elevation for true (**D**), xz'y'' (**E**), yx'y'' (**F**), and swing-spin (**G**) GH axial rotation. The left column portrays the axial orientation plots for xz'y'' (**A**), yx'y'' (**B**), and swing-spin (**C**) from which apparent axial rotation was derived. The singular data points indicate axial orientation/rotation at minimum/maximum HT elevation (differs by subject). The errors bars around the singular data point and the shaded regions indicate ±1 standard deviation. The black solid line at the top of plots on the right column indicates regions where a SPM1D one-way repeated-measures ANOVA test found a difference in axial rotation between planes of elevation (CA, SA, FE) – a suprathreshold event. The following suprathreshold events exceeded $p \leq 0.001$: swing-spin between 25°-78° of HT elevation ($p=0.006$), and beyond 128° of HT elevation ($p=0.050$). The colored solid lines (green for CA, purple for SA, and orange for FE) at the top of plots on the right column indicate regions where a SPM1D non-parametric t-test found significant differences from 0° of axial rotation. The following suprathreshold events exceeded $p \leq 0.001$: true axial rotation for SA ($p=0.002$), xz'y'' for SA between 122°-130° of HT elevation ($p=0.02$), swing-spin for FE ($p=0.002$).

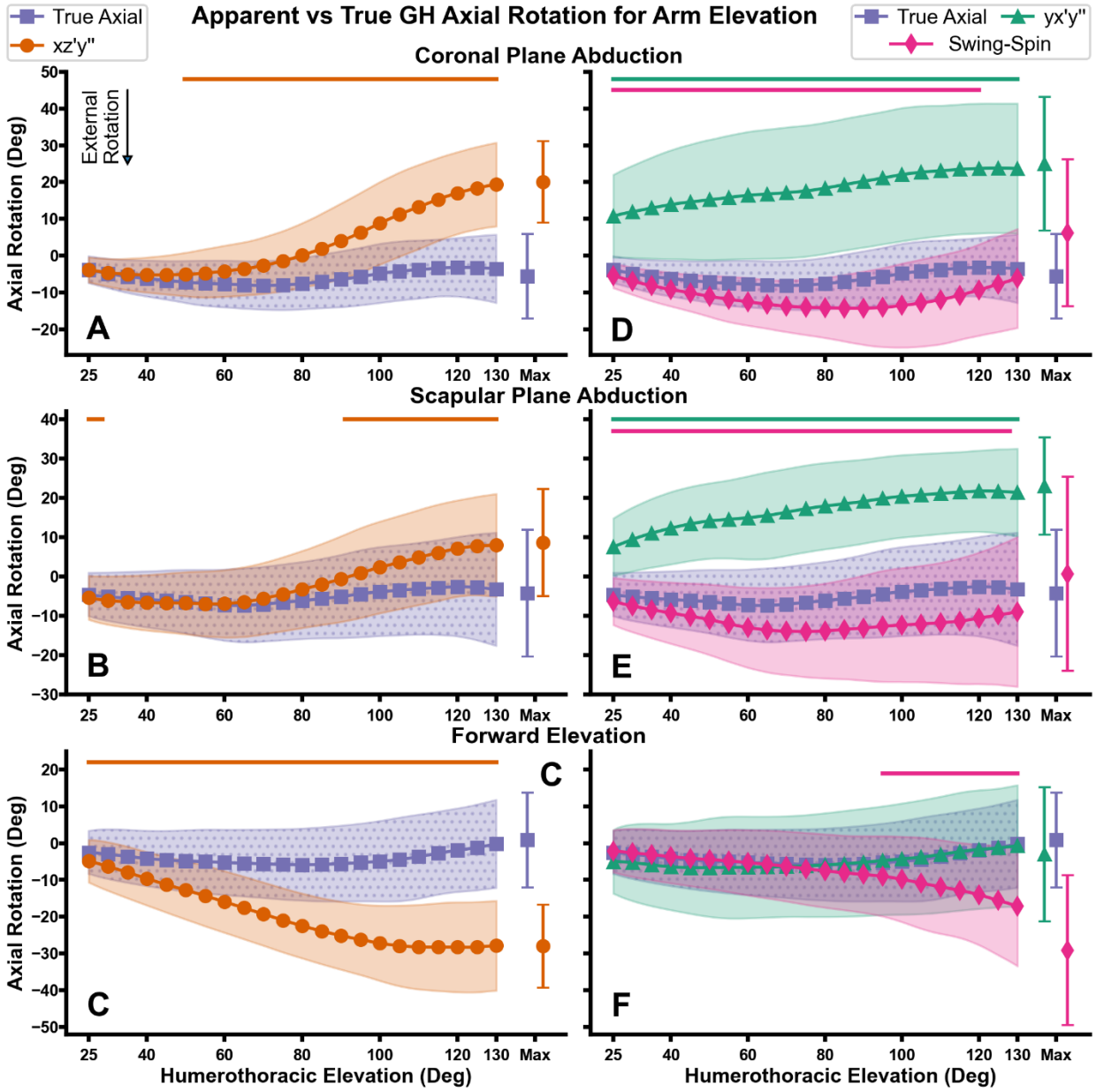

Fig. 4: Comparison of xz'y'' (**A-C**), yx'y'', and swing-spin (**D-F**) apparent GH axial rotation versus true GH axial rotation for CA (**A, D**), SA (**B, E**), and FE (**C, F**). The singular data point indicates axial rotation at maximum HT elevation (differs by subject). The errors bars around the singular data point and the shaded regions indicate ±1 standard deviation. The solid lines (orange for xz'y'', green for yx'y'', and magenta for swing-spin) at the top of each plot indicate regions where a SPM1D non-parametric paired t-test found significant differences between apparent and true axial rotation. The following suprathreshold events exceeded p≤0.001: xz'y'' for SA between 25°-29° of HT elevation (p=0.020), and between 91°-130° of HT elevation (p=0.003).

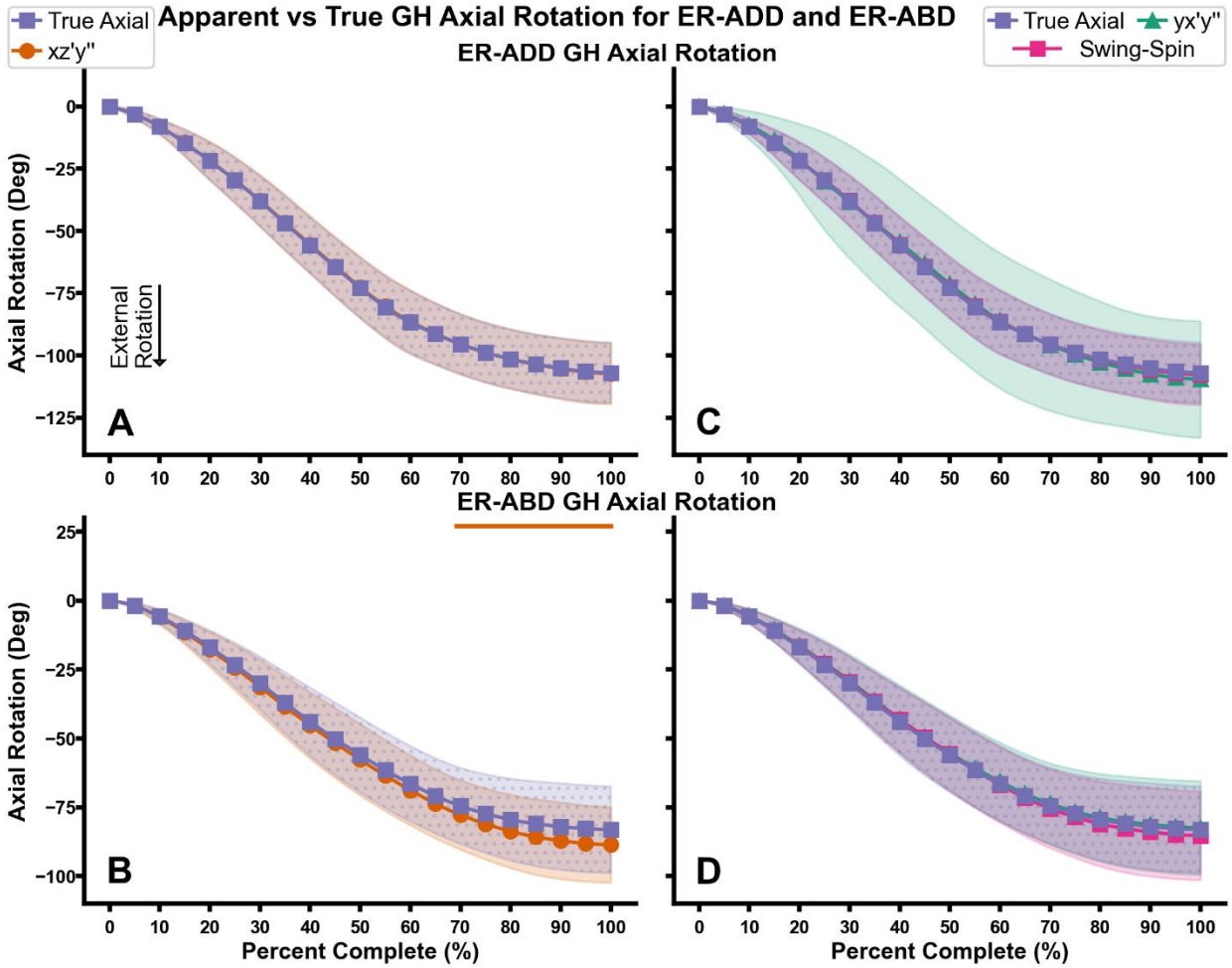

Fig. 5: Comparison of xz'y'' (**A, B**), yx'y'', and swing-spin (**C, D**) GH apparent axial rotation versus true GH axial rotation for ER-ADD (**A, C**) and ER-ABD (**B, D**). Trials were interpolated at 0.25% increments between the start (0%) of the motion and maximum external rotation (100%). The shaded regions indicate ±1 standard deviation. The solid lines (orange for xz'y'', green for yx'y'', and magenta for swing-spin) at the top of each plot indicate regions where a SPM1D non-parametric paired t-test found significant differences between apparent and true axial rotation. The following suprathreshold events exceeded p≤0.001: xz'y'' for ER-ABD beyond 70% of motion completion (p=0.002).

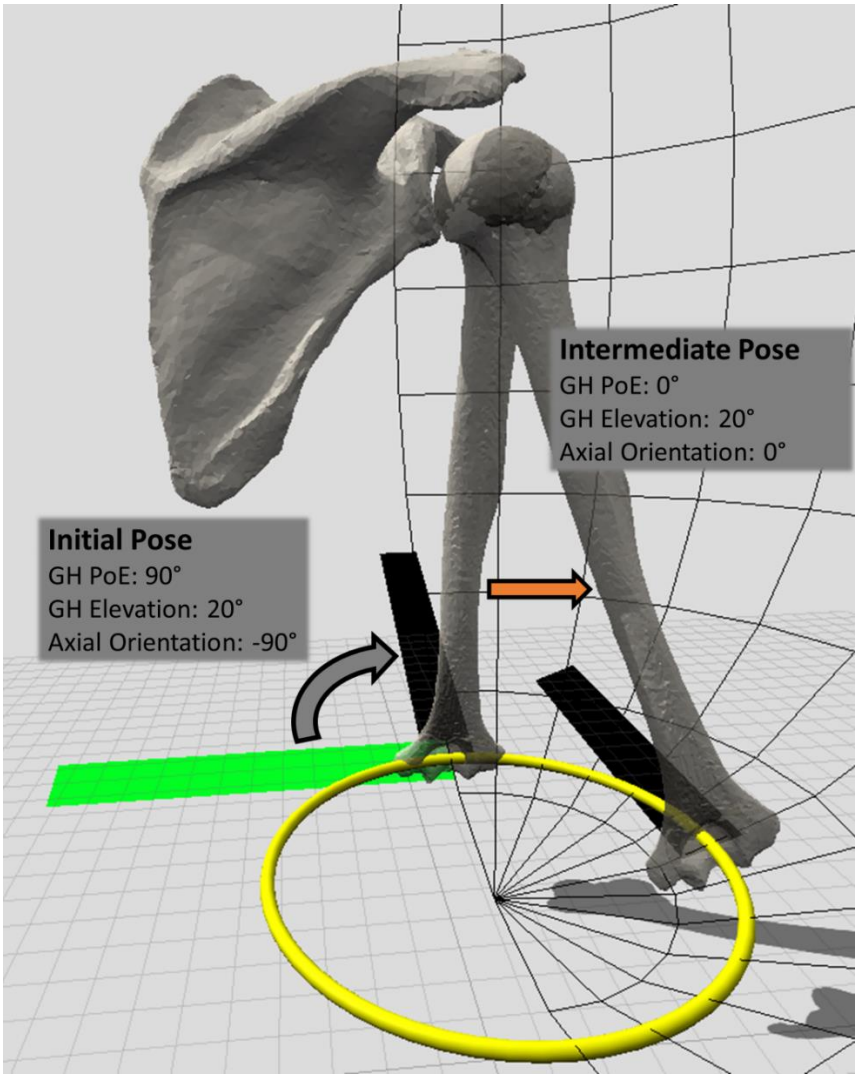

Fig. 6: Illustration of how changes in PoE affect axial rotation as measured by the yx'y'' sequence during CA, with the forearm (black rectangle) pointing anteriorly. Because of body habitus and posture, in the initial pose the humerus is slightly elevated (20°) in the sagittal plane. Since for the yx'y'' sequence axial orientation is measured from an axis (green) that is tangent to the latitude (yellow circle), one would measure 90° of external axial orientation. As the subject elevates in the coronal plane, with the forearm still pointing anteriorly, they arrive at 20° of GH elevation in the coronal plane. Here the forearm is already colinear with the axis that is tangent to the latitude (yellow circle), therefore one would measure 0° of axial orientation. Hence, between these two poses, apparent axial rotation dictates that the humerus underwent 90° of internal axial rotation – which does not correspond to the actual rotation about the humerus' longitudinal axis.